APPLIED AND ENVIRONMENTAL MICROBIOLOGY, Oct. 1988, p. 2464–2471 Vol. 54, No. 10
0099-2240/88/102464-08$02.00/0

Product Inhibition of Immobilized *Escherichia coli* Arising from Mass Transfer Limitation

PHILIP S. STEWART AND CHANNING R. ROBERTSON*

Department of Chemical Engineering, Stanford University, Stanford, California 94305-5025

Received 20 May 1988/Accepted 19 July 1988

Mass transfer-limited removal of metabolic products led to product-inhibited growth of *Escherichia coli* that was immobilized in a model system. Comparison of the growth kinetics of immobilized and free-living cells revealed no further physiological differences between cells in these two modes of existence beyond those manifested in the local concentrations of substrate and product. Bacteria were retained on a microporous membrane in a dense, planar aggregate and were grown anaerobically on a glucose-based minimal medium. Radioisotope labeling of the immobilized cell mass with ^{35}S was used to determine growth kinetic parameters. Growth rates in the immobilized cell layer were measured by an autoradiographic technique which allowed comparison of the size of the growing region with the rate of cell convection caused by growth. Immobilized cell growth rates and growth yields ranged from near maximal (0.56 h^{-1} and 39 g of dry cell weight/mol of glucose, respectively) to substantially reduced (0.15 h^{-1} and 15 g/mol). The depression of these kinetic parameters was attributed to product inhibition arising from mass transfer-limited removal of acidic waste products from the cell mass. A simple one-dimensional reaction-diffusion model, which incorporated data on the product-inhibited growth kinetics of free-living cells collected in a product-limited chemostat, satisfactorily predicted product inhibition of immobilized cell growth.

The reactivity of a microbial biofilm, floc, or synthetically immobilized preparation (all of which are generally referred to as immobilized cell aggregates) is crucially linked to the intrinsic kinetic behavior of the microorganisms. Understanding of the intrinsic kinetic behavior in these systems is not straightforward, however, since changes in the local cellular environment often accompany immobilization. Immobilized microbial kinetic behavior may therefore differ significantly from the behavior that would be anticipated for free-living cells under the bulk solution conditions. Physical mechanisms which could plausibly effect changes in the local environment include electrostatic partitioning of charged species between the cell aggregate and the free solution, concentration gradients arising from diffusion-limited mass transport of reacting species, and physical or chemical interactions between cells and the support matrix. In view of these diverse processes and the complex nature of microbial growth, it is not surprising that there have been a number of reports in which altered behavior of immobilized cells has been described. These have been reviewed briefly elsewhere (6, 8).

The significance of mass transfer limitation of substrate transport in particular has been widely recognized and documented (12, 17). In this study we explored a second potential consequence of diffusional limitation, namely, the attainment of inhibitive levels of metabolic waste products within the cell aggregate. Product inhibition of microbial activity is a common phenomenon, especially in anaerobic or anoxic systems. When a microorganism that is susceptible to product inhibition is immobilized, product inhibition effects are likely to be exacerbated by the diffusional limitation on the egress of products. It is important to recognize that, because of the steep concentration gradients that often prevail in immobilized cell systems, product inhibition may be a consideration even when the bulk solution product concentration is well below the inhibitive level.

* Corresponding author.

Product inhibition arising from mass transfer limitation can be analyzed within the framework of an appropriate reaction-diffusion model. Indeed, several models of immobilized enzyme and cell activity which account for product inhibition have been described (2, 3, 18, 21). The principal aim of these treatments has been to develop expressions that describe the overall rate of reaction in systems in which diffusion and reaction are both important. The focus of the present study was to apply simple results from reaction-diffusion theory in order to elucidate the biological consequences of mass transfer limitation, in particular, with respect to product inhibition.

There is some experimental evidence for mass transport-induced product inhibition in immobilized cell systems. Depressed reaction rates have been attributed to product inhibition in a few instances (5, 7, 21, 23). A more graphic indication of mass transfer limitation of product removal is revealed by direct measurement of gradients in product concentrations between the cell aggregate and the bulk solution. Hydrogen ion concentration gradients established across active biofilms have been documented by comparing the pH at the base of a biofilm with the bulk pH. In a denitrifying biofilm, reaction-generated alkalinity can lead to a pH in the interior of the biofilm that is up to 2 pH units higher than that in the bulk solution (1). Conversely, in a nitrifying biofilm reaction, generated acidity leads to a substantially lower pH in the biofilm than in the bulk solution (22). As these investigators have pointed out, such modifications of the local environment within the biofilm may lead to changes in the intrinsic kinetics.

The intent of this study was to demonstrate product inhibition of immobilized cell growth in a model immobilized cell system. Because product inhibition is difficult to diagnose from measurements of the overall reaction rate, we sought measurements of the intrinsic kinetic behavior that are independent of the mass transfer characteristics of the system. Radioisotope labeling methods developed in this laboratory (11; S. F. Karel and C. R. Robertson, submitted

for publication) were used to characterize the growth kinetics (the growth rate, μ, and the growth yield, Y_{xs}) of a model immobilized bacterial system. Elementary results from the theory of reaction and diffusion in permeable media were applied in order to compare the kinetic behavior of immobilized and suspension-cultured cells.

MATERIALS AND METHODS

Nomenclature. The following variables and constants are used in this paper: a, dimension of growing zone; A, substrate-supplied surface area of cell aggregate; b, observed autoradiographic band width; b', corrected band width; d, characteristic resolution distance; D_j, solution diffusivity of species j; L, dimension of cell aggregate; P, product concentration; P_i, product concentration at which substrate uptake ceases; q_j, specific reaction rate of species j; R_j, overall reaction rate of species j; S, substrate concentration; t_c, duration of chase period; t_p, duration of pulse period; w, dimensionless product concentration; x, autoradiographic band separation; X, aggregate cell density; Y_{jk}, yield coefficient of species j on species k; z, extent of autoradiographic image; μ, average specific growth rate in the growing zone; μ^*, growth rate estimated from overall rate. The following subscripts are used: e, concentration at substrate-exhausted edge; j,k, arbitrary; m, concentration in the medium; o, concentration in the bulk solution; p, product; s, substrate; t, tracer; x, biomass.

Culture conditions. *Escherichia coli* B, ATCC 11303, was obtained from the American Type Culture Collection (Rockville, Md.). Inocula were grown aerobically on 8 g of nutrient broth (Difco Laboratories, Detroit, Mich.) per liter. Bacteria were otherwise cultured anaerobically at 37°C on a phosphate-buffered minimal medium with glucose as the sole carbon and energy source. The initial medium pH was 7.4. The complete medium contained Na_2HPO_4, 5.0 g/liter; KH_2PO_4, 1.0 g/liter; NH_4Cl, 2.0 g/liter; Na_2SO_4, 0.5 g/liter; $MgSO_4 \cdot 7H_2O$, 50 mg/liter; $CaCl_2$, 2 mg/liter; $NaHCO_3$, 42 mg/liter; $FeSO_4 \cdot 7H_2O$, 1 mg/liter; $MnSO_4 \cdot H_2O$, 1 mg/liter; $ZnSO_4 \cdot 7H_2O$, 1 mg/liter; and glucose, 0.90 to 3.60 g/liter. For the radiolabeling of immobilized cells with ^{35}S, the amount of Na_2SO_4 was reduced to between 5.7 and 18.2 mg/liter, and all other sulfate salts were supplied as the corresponding chlorides at 1 mg/liter. This formulation ensured that sulfur was present in at least 1.5 times excess over the amount of glucose. Carrier-free $H_2{}^{35}SO_4$ (ICN Pharmaceuticals Inc., Irvine, Calif.) was added to give a final specific activity of 20 mCi of sulfur per mmol. Buffer contained Na_2HPO_4, 5.0 g/liter; KH_2PO_4, 1.0 g/liter; NH_4Cl, 2.0 g/liter; and Na_2SO_4, 0.5 g/liter. All media were sterilized by filtration through a 0.22-μm-pore-size filter (Millipore Corp., Bedford, Mass.).

Batch and continuous culture studies of free-living cell growth and metabolism were carried out in a 2-liter benchtop fermentor (Setric). The fermentor and ancillary tubing were sterilized by autoclaving them prior to each run. Oxygen was excluded by maintaining a slight positive pressure of N_2 in the headspace above the culture or by sparging the culture with 5% CO_2 in N_2. The gas in either case was humidified and filter sterilized upstream of the fermentor. In order to investigate product inhibition, the fermentor was operated as a product-limited chemostat by omitting the pH control and supplying a surplus of glucose in the medium. In this mode, the growth rate of the culture was attenuated by the attainment of inhibitive levels of acidic products rather than by the depletion of a substrate. The effluent pH ranged from 5.9 to 6.7 in these experiments. The long-term behavior of the chemostat was characterized by a slow drift or oscillation in the optical density of the culture, with little change in effluent pH. Data were collected after periods of 4.5 to 7 times the inverse dilution rate.

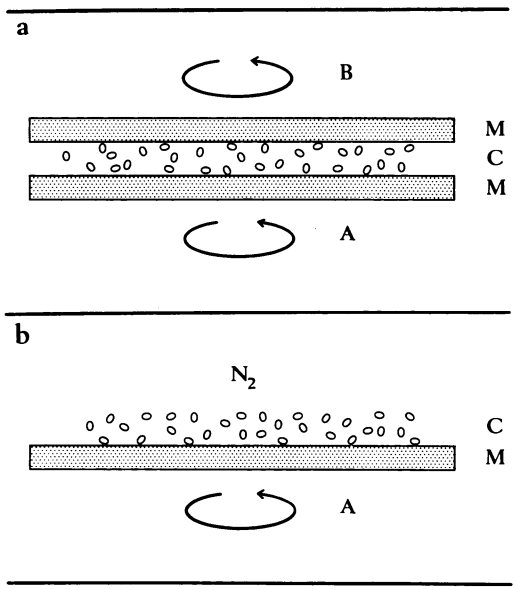

FIG. 1. Immobilized cell reactor. The cell mass, C, is retained by microporous membranes, M. Medium circulates continuously through chamber A. (a) Chamber B is filled with buffer and sealed. (b) Nitrogen gas fills the chamber above the cell layer.

Immobilized cell reactor. Bacteria were immobilized by retention in a planar layer between two microporous cellulose membranes (pore size, 2 μm; type GS; Millipore). The membranes and cell layer were housed in a reactor body that was machined from cast acrylic. This design, depicted schematically in Fig. 1a, allowed access to cylindrical compartments (1 to 2 cm^3) on either side of the cell layer. Both compartments were magnetically stirred to facilitate mass transfer, and each was fitted with inlet and outlet ports. Medium, buffer, or fixative was supplied continuously to one chamber, while the other was ordinarily sealed to prevent convective flow across the cell layer. The entire reactor could be immersed in a thermostated water bath to provide temperature control. The total surface area available for bacterial growth was 3.0 cm^2.

A modification of this design, in which one membrane was omitted and the adjacent chamber was filled with nitrogen gas, was used for experiments requiring radioisotope labeling (Fig. 1b). This configuration facilitated rapid equilibration of the tracers that were introduced in the liquid phase throughout the cell mass. Elimination of the potential volume constraint of cell growth imposed by the second membrane also helped to ensure a temporally uniform cell density. Gaseous products of bacterial metabolism were vented to the atmosphere through a water trap which provided a back pressure of 5 to 10 cm of H_2O. This scheme afforded a homogenous cell mass with well-defined boundaries.

The reactor was sterilized prior to each experiment by treatment with 2% formaldehyde followed by a flush with sterile water. An inoculum of 3 to 10 mg of cells was deposited on the membrane by filtration. This corresponded to a cell layer depth of approximately 50 to 125 μm. The cellulose membrane was supported by a stainless steel screen during the filtration step. Immediately following this

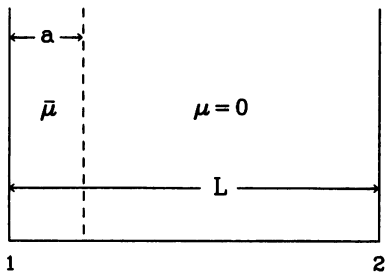

FIG. 2. Geometry of the cell aggregate. Cell growth occurred only in a limited region of dimension a, which was less than the total extent of the aggregate, L. The substrate-supplied edge is denoted by 1, and the substrate-exhausted edge is denoted by 2.

step, the screen was removed and the membrane supporting the inoculum was refitted into the reactor.

Measuring concentration gradients. For clarity in the following explanation, the two boundaries of the cell layer are referred to as the substrate-supplied and substrate-exhausted edges. Acid concentrations at the substrate-exhausted edge were measured by allowing the sealed, buffer-filled chamber contiguous with that edge to reach equilibrium. Chamber A (Fig. 1a) was supplied continuously with medium, and sealed chamber B was filled with buffer that lacked any carbon source. After the system was allowed to achieve steady state (8 to 10 h), the contents of chamber B were removed and analyzed.

Autoradiographic determination of local growth rates. An estimate of the local growth rate can be obtained by comparing the rate of cell convection in the aggregate with the dimension of the growing zone. Both of these measurements may be extracted by autoradiographic examination of a cell aggregate which has been labeled in a pulse-chase-pulse sequence. To illuminate this approach, consider the growth of cells within a planar aggregate, as depicted in Fig. 2. Cell growth is assumed to be limited to a region of fixed depth, a, which is less than the total extent of the aggregate, L. Cells outside this zone are nongrowing. Provided there is no sloughing or other loss of biomass, the total depth of the biofilm increases as cell mass accumulates. Assuming that the cell density is constant throughout the aggregate, the velocity with which cells in the nongrowing region are convected away from the substrate-supplied edge of the cell aggregate is given simply by μa, where μ is the average specific growth rate in the growing region.

Now, suppose that the cell aggregate is labeled with pulses of equal duration, t_p, which are separated by a chase period of duration t_c. This protocol results in two bands of labeled cell mass, which will be spatially separated because of the convection that occurs during the chase and second pulse periods. The distance traveled by the substrate-exhausted edge of the first pulse is $x = \mu a(t_c + t_p)$. The local growth rate can thus be estimated from such an experiment, provided that one can measure the band separation, x, and the characteristic dimension of the growth zone, a. Absolute measures of these two distances are not necessary, since only their ratio is required to calculate a growth rate.

The most challenging aspect of this scheme is obtaining an accurate estimate of the dimension of the growing zone depth, a. Imperfect autoradiographic resolution and growth during the pulse period both contribute to broadening of the observed band width with the experimental approach that we used. Corrections for both of these effects can be formulated. Loss of autoradiographic resolution arises principally from the fact that the radioactive label is not truly coplanar with the film emulsion, since the specimen section and the film emulsion both have a finite thickness. For a square wave activity distribution, the observed band width at the peak half-height, b, is related to the actual band width, b', by $b = (b'^2 + 4d^2)^{1/2}$, where d is a characteristic resolution distance (20). In this study, d was taken as the average of the section and emulsion layer thicknesses. The thickness of the dried emulsion layer was estimated by parting the layer at a 45° angle with a razor blade and examining the cut under a microscope. Growth during the pulse period can be corrected for by considering local material balances on labeled biomass (Karel and Robertson, submitted). Broadening of the band width at the peak half-height is given approximately by $b' = (1 + \mu t_p/2)a$. The actual depth of the growing zone can then be estimated from the following equation: $a = (b^2 - 4d^2)^{1/2}/(1 + \mu t_p/2)$. Measurement of b and x from autoradiographs is described below.

A second estimate of the local growth rate can be made by comparing the dimension of the growth zone with the overall rate of tracer uptake: $\mu^* = R_t Y_{xt}/aAX$. In this equation, R_t is the overall rate of tracer uptake, Y_{xt} is the yield of biomass on tracer, A is the reactive surface area, and X is the aggregate cell density. Because of the error inherent in measuring R_t precisely at low conversions, this approach is less accurate than the purely autoradiographic one described above, but it does afford an assessment of the self-consistency of the experimental measurements.

Radiolabeling protocol. Radiolabeling experiments were carried out with the reactor configured as shown in Fig. 1b. Following inoculation as described above, the reactor was supplied continuously with medium, either unlabeled or labeled, at a fixed flow rate for the duration of the experiment. The reaction rate, as reflected in the effluent pH, was essentially constant over the course of the experiment, with the exception of a 2- to 5-h transient initiation period. In experiments designed to measure growth rates or growing zone depths, a pulse-chase-pulse-fix or pulse-fix radiolabeling protocol was initiated only after the effluent pH attained a steady state. It is important in these experiments that the duration of the pulse be sufficiently longer than the characteristic mixing and diffusion times. At the flow rates used in the pulse-labeling experiments, the residence time in the medium chamber of the reactor was 3 to 6 min. The time scale for diffusion into the cell aggregate (L^2/D) is likewise estimated to be on the order of magnitude of a few minutes. Labeled medium was always provided in 1-h pulses. The chase period lasted from 10 to 24 h. Fixative was introduced into the reactor immediately following the end of the final labeling pulse, quenching further growth and preserving the spatial distribution of label. In experiments intended to measure the growth yield, labeled medium was supplied continuously to the reactor. Multiple measurements of sulfur uptake and glucose consumption were made over a 3-h period after steady state was achieved.

Autoradiography. The labeled cell mass was fixed and embedded as described below for electron microscopy, but with the omission of OsO_4 postfixation and uranyl acetate staining. Cross-sections through the cell layer, 1 to 2 μm thick, were deposited on gelatin-coated glass slides, dip coated with nuclear track emulsion (NTB-3; Eastman Kodak Co., Rochester, N.Y.), air dried at room temperature, and then exposed in light-tight slide boxes for 48 to 400 h at 4°C. Autoradiographs were developed in half-strength D-19 developer (Kodak) for 3 to 5 min, rinsed in distilled water for

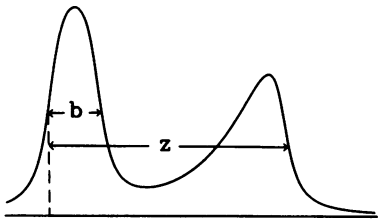

FIG. 3. Illustration of autoradiographic measurements.

15 s, fixed (Kodak Ektaflo fixer) for 8 min, and finally rinsed again in water for 15 min. After air drying, silver grain patterns were examined under the microscope with bright-field illumination. Autoradiographs were photographed with a positive-negative film (Polaroid 55).

Negatives (4 by 5 inches [10.2 by 12.7 cm]) were digitized and analyzed by using a video image acquisition system. The signal-to-noise ratio was improved by averaging data from a single negative in a direction parallel to the plane of the cell layer, as defined by the autoradiographic bands. Two measurements were extracted from pulse-chase-pulse autoradiographs, as illustrated in Fig. 3. The apparent band width, b, was defined as the width at the peak half-height of the band corresponding to the final labeling pulse. The extent of the autoradiographic image, z, was defined as the horizontal distance between the respective points of half-maximal density of the two peaks making up the autoradiograph. The measurement was made from the substrate-exhausted edge of the peak corresponding to the first pulse to the substrate-supplied edge of the peak corresponding to the final pulse. The band separation, x, was then taken as $z - b$.

Electron microscopy. The cell layer was cross-linked in place in the reactor with a fixative made up of glutaraldehyde, 20.0 g/liter; Na_2HPO_4, 5.0 g/liter; KH_2PO_4, 1.0 g/liter; and NaCl, 2.0 g/liter. After several hours of in situ fixation, the membrane and cell layer were removed from the reactor as a unit. The sample was postfixed with 2% osmium tetroxide in buffer, stained with 1% uranyl acetate, dehydrated in an ethanol series, and then embedded in an ultra-low-viscosity resin (Polysciences). Thin sections (60 to 90 nm) were poststained with lead citrate and examined with a transmission electron microscope (Philips 410).

Assays. Cell mass was determined as dry weight. Portions of 50 ml of fermentation broth were centrifuged (3,000 × g, 15 min), and the cell pellet was quantitatively transferred with a water wash to a 1.5-ml minicentrifuge tube. The cells were again pelleted (8,000 × g, 4 min), the supernatant was removed by aspiration, and the tubes containing the cell pellets were dried at 70°C for 48 to 72 h to constant weight. The tube tare was obtained by removing the dried cell material from the tube and reweighing. Glucose was determined enzymatically (Sigma Chemical Co., St. Louis, Mo.). The total acid concentration was quantified through pH measurement by comparison with a titration curve of the medium. Individual acid species were assayed by high-pressure ion-exclusion chromatography with UV detection. The separation was performed with a cation-exchange column (Polypore H; Brownlee), with 0.01 N H_2SO_4 as the mobile phase. Sodium azide, at 0.5 g/liter, was used as an internal standard. Sulfur was determined in ^{35}S-radiolabeled samples by liquid scintillation counting (LS3801; Beckman Instruments, Inc., Fullerton, Calif.). Samples were diluted 1:9 with a commercial scintillation cocktail (PCS II; Amersham Corp., Arlington Heights, Ill.).

RESULTS AND DISCUSSION

Free-living cell kinetics. Data characterizing the product-inhibited growth of free-living *E. coli* are summarized in Table 1. Product inhibition effects were correlated in terms of a single variable, the total acid concentration. This approach is tenable only because all of the experiments were conducted in media with the same buffer composition. It is thought that, in general, acid inhibition of bacterial growth is caused by the accumulation of the protonated form of a weak acid, which acts as an uncoupler to dissipate the proton gradient across the cell membrane (10, 16). Acid inhibition would therefore be a function not only of the total acid concentration but also of pH. It also depends on the relative proportions of acidic species if they have different pK_a's. While acknowledging the probable complexity of acid inhibition, it is a convenient simplification in this case to correlate growth kinetics solely in terms of the total acid concentration.

The specific growth rate and yield of cellular dry matter on glucose both decline with increasing acid concentration. The ratio of these two kinetic parameters, the specific substrate uptake rate, q_s, also decreases monotonically with increasing acid concentration (Table 1). The product concentration at which substrate uptake ceases, P_i, is found by extrapolating the data for q_s to the x intercept (P_i = 33 mM). This value has no general significance since it is highly dependent on both the buffer capacity and the initial pH of the medium. Product concentrations reported hereafter were normalized by dividing by P_i.

During anaerobic growth on glucose, *E. coli* carries out a mixed acid fermentation, producing a mixture of simple organic acids (9). The principal products found in this study were formate and acetate, appearing in approximately a 2:1 ratio, respectively, with lesser amounts of lactate, succinate, and pyruvate being present (data not shown). Two shifts in the spectrum of products were evident as the acid concen-

TABLE 1. Summary of free-living cell growth kinetics

μ (h^{-1})	Y_{xs} (g/mol)	Y_{ps} (mol/mol)	q_s (mmol/g per h)	P (mM)	P/P_i	Culture method[a]
0.67	34.0	2.35	19.7	1.0	0.03	a
0.56	31.0	2.44	18.1	14.2	0.43	b
0.52	34.4	2.53	15.1	19.1	0.58	c
0.43	29.2	2.41	14.7	17.8	0.54	b
0.31	26.4	2.34	11.7	21.7	0.66	b
0.14	24.9	1.94	5.6	26.8	0.81	b
0.086	16.7	2.04	5.2	26.8	0.81	c
0.052	9.6	2.03	5.4	28.9	0.88	b

[a] Culture methods were as follows: a, batch with N_2 purge; b, chemostat with N_2 purge; c, chemostat with 5% CO_2 in N_2 sparge.

tration increased, both of which tended to reduce the total acid yield. Less formate and more CO_2 appear, presumably reflecting an increased activity of formate hydrogen lyase (4). A second effect which may contribute to the diminished acid yield at lower pH is a shift toward increased formation of lactate and less formation of acetate and formate. The maximum theoretical yield of lactate on glucose is 2 mol/mol, while the maximum combined yield of formate and acetate is about 3 mol/mol. The net effect of these changes is that the total soluble acid yield is reduced from about 2.4 mol/mol of glucose under noninhibited conditions to about 2.0 mol/mol under product-inhibited conditions.

Sulfur was used as a tracer for the estimation of biomass in this study. Sulfur was incorporated principally into cellular proteins and was released only very slowly under the conditions used in this study. It is a suitable measure of cell mass because the yield of biomass on sulfur is expected to be relatively independent of growth conditions, provided that sulfur itself is not growth limiting. The yield of biomass on sulfur, as measured in a batch experiment which traversed a range of acid concentrations, was 6.8 ± 0.3 g/mmol of sulfur. This value was used to convert substrate yields based on sulfur to yields based on dry mass.

Product concentration in the cell aggregate. A prerequisite for assessing the role of product inhibition in dictating immobilized cell kinetics is an estimate of the local product concentration within the immobilized cell aggregate. This concentration can be predicted theoretically by using an appropriate model of reaction and diffusion in the microbial aggregate (12). Consider a microbial aggregate in which reactivity may be approximated by a single reaction converting a substrate to an inhibitory product with a molar yield coefficient of product on substrate of Y_{ps}. At any point of substrate exhaustion, the product concentration can be expressed as

$$w_e = P_e/P_i = (D_s Y_{ps} S_o/D_p P_i) + P_o/P_i \quad (1)$$

where P_e and w_e are the respective dimensional and dimensionless product concentrations at this point. D_s and D_p are the respective solution effective diffusivities of the substrate and product, and S_o and P_o are the respective bulk concentrations of these species. In deriving this expression, it was assumed that there was no differential partitioning of either substrate or product between the cell aggregate and free solution and that the ratio of the effective diffusivity in the aggregate relative to the solution diffusivity was the same for both species. The product concentration was normalized by comparison with an inhibitive product concentration, P_i, defined as described above.

The parameter w_e affords a quantitative upper bound on the extent of product inhibition that may occur in an immobilized cell system that is independent of the specific kinetic behavior or mass transfer characteristics of the system. When $w_e \ll 1$, the product concentration within the aggregate is well below the inhibitive product concentration, so product inhibition effects can be neglected. When $w_e \approx 1$, product inhibition is significant. Calculation of w_e offers a simple, design-independent means of estimating the magnitude of product inhibition effects in an immobilized cell system.

In any system in which the substrate concentration in the aggregate approaches zero, w_e provides a reasonable first-order approximation of the product concentration that is prevailing in the active zone. This may be seen by considering the limiting case of zero-order kinetics. One finds, in this case, that the average product concentration in the active zone is 2/3 w_e in the absence of external mass transfer resistance and approaches w_e identically as external mass transfer resistance becomes increasingly important. Therefore, in any system in which the substrate is exhausted within the cell aggregate, w_e never overestimates the average local product concentration by more than 50% and becomes increasingly more accurate as external mass transfer resistance becomes more pronounced. We chose to correlate product inhibition effects in immobilized cells by calculating w_e. The appeal of this approach is that it does not rely on particular numerical values of the effective diffusivity in the cell aggregate and the external mass transfer coefficient, parameters that are difficult to measure precisely or independently.

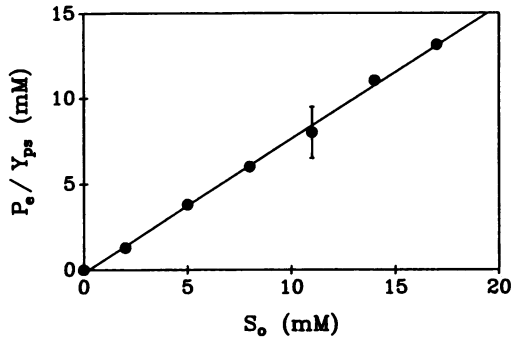

FIG. 4. Coupling between the bulk substrate concentration and the product concentration in equilibrium with the substrate-exhausted edge.

Direct measurements of the total acid concentration in equilibrium with the substrate-exhausted edge of an active cell mass are reported graphically in Fig. 4. These experiments were performed at low conversions, so that $P_o \approx 0$. Referring, then, to equation 1, a plot of P_e/Y_{ps} versus S_o should yield a curve whose slope is equal to the ratio of the substrate and product diffusivities, D_s/D_p. The linearity of the experimental data suggests that D_s/P_p is essentially constant, with a value of 0.78 ± 0.05. This value lies between the calculated ratios obtained by considering the solution diffusivities of either of the principal product or buffer species (Table 2). This result reflects the fact that the motion of the products, which exist principally in the dissociated state, is coupled electrostatically and through reaction to the motion of the buffer components $H_2PO_4^-$ and HPO_4^{2-} (19). The data demonstrate the applicability of equation 1 and confirm that significant product concentrations can be attained in the cell aggregate.

Immobilized cell kinetics. An electron micrographic cross-section of a cell layer is reproduced in Fig. 5. Qualitative visual inspection suggested that the boundaries of the aggregate are well defined and that the cell density is approxi-

TABLE 2. Diffusivities of principal species in water at 25°C

Species	D_j (cm²/s)	D_s/D_j
Glucose	6.9×10^{-6}[a]	1.00
Formate	1.45×10^{-5}[b]	0.48
Acetate	1.09×10^{-5}[b]	0.63
$H_2PO_4^-$	8.78×10^{-6}[c]	0.79
HPO_4^{2-}	7.58×10^{-6}[c]	0.91

[a] See reference 15.
[b] See reference 19.
[c] See reference 14.

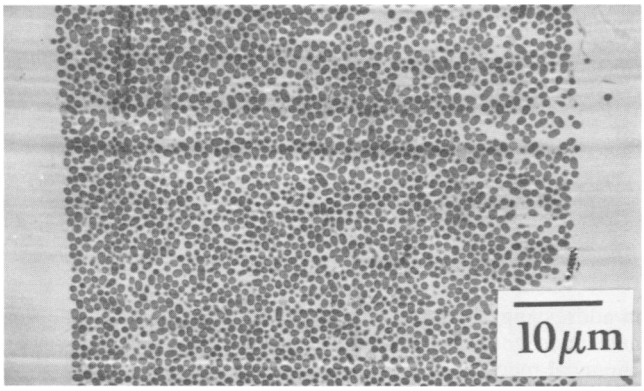

FIG. 5. Electron micrograph of cell layer in cross-section.

mately uniform throughout the layer. The volume fraction occupied by cells in the aggregate was estimated by point counting with correction for the section thickness to be about 75% (24). If the specific volume of the *E. coli* cell is taken to be 2.91 ml/g (P. S. Stewart and C. R. Robertson, submitted for publication), an aggregate cell density of about 260 g/liter is implied. Cell aggregates were typically 100 to 250 μm in depth at the end of an experiment.

An autoradiograph prepared from a pulse-chase-pulse labeling experiment and the averaged intensity profile obtained from this image are reproduced in Fig. 6. In this and other autoradiographs, the silver grain band corresponding to the final labeling pulse was always well defined spatially, although it was not necessarily uniform in intensity across its breadth. The silver grain band corresponding to the initial labeling pulse was always slightly shorter than the final band as a result of dilution of the local tracer activity by growth as the labeled cells were convected out of the growing zone. A faint third band is visible in this autoradiograph, coinciding with the substrate-exhausted edge of the cell layer. Activity at this point in the cell aggregate could have been due to aerobic growth on an acid product (e.g., acetate), provided that a residual amount of oxygen was present in the gas-filled chamber. Sulfur incorporation at the substrate-exhausted edge provides circumstantial evidence that the tracer penetrates the entire cell layer during the pulse period.

The autoradiographic data, together with derived estimates of the depth of the growth zone and the local growth rate, are summarized in Table 3. Note that the only experimental parameter that varied in these experiments was the bulk substrate concentration. High cell densities and the significant external mass transfer resistance imposed by the membrane and adjacent convective boundary layer restricted growing zones to 30 μm or less. The depth of the growing zone expanded as the bulk substrate concentration was increased. The average local growth rate in the cell aggregate decreased as the substrate concentration was increased, from near maximal to less than 20% of the maximum growth rate measured in batch culture. This behavior is inconsistent with substrate limitation of growth. Rather, it may be interpreted as reflecting higher local concentrations of acidic products in the aggregate when media with higher substrate concentrations were used. In qualitative terms, the extent of the active region of the aggregate was determined by transport of the substrate, and kinetic behavior within the active zone was dictated by the local concentration of product.

In order to make a graphic comparison of free-living and immobilized cell growth behavior, local product concentrations in the immobilized cell aggregate were estimated by using equation 1. It should be pointed out that the bulk product concentration was never substantially inhibitive in the immobilized cell experiments ($w_o \leq 0.27$ for growth yield measurements and $w_o \leq 0.10$ for growth rate measurements). Growth rates and growth yields of free-living and immobilized cells are presented in Fig. 7. Immobilized cell kinetic behavior was satisfactorily predicted by the simple reaction-diffusion model. Modest overestimation of the growth yield coefficient of immobilized bacteria may have been due to a small amount of oxygen reaching the cell mass, either in the feed stream or via the gas-filled volume contiguous with the substrate-exhausted edge of the cell layer.

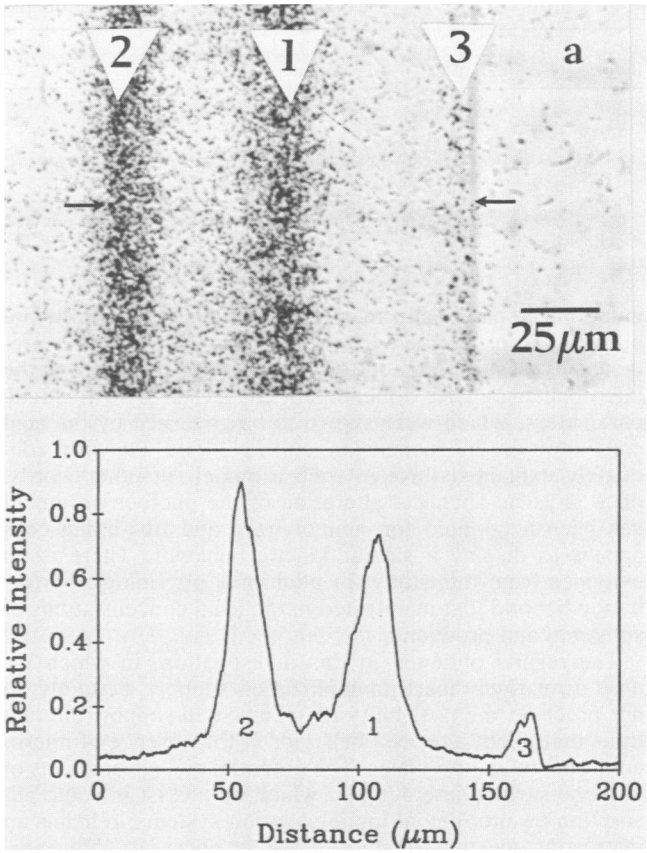

FIG. 6. (a) Autoradiograph resulting from a pulse-chase-pulse labeling experiment. The first band of labeled biomass (band 1) was convected away from the growing region. Because the sample was fixed immediately following the second pulse, the band corresponding to this pulse (band 2) delimited the growth zone, which was contiguous with the substrate-supplied edge of the cell aggregate. A faint third band (band 3) coincided with the substrate-exhausted edge of the cell mass. Arrows indicate the estimated extent of the aggregate. (b) Averaged intensity profile of the autoradiograph shown in panel a. The units of intensity are arbitrary. The peaks are numbered to indicate labeling pulse correspondence.

Summary. Results of these experiments demonstrate that product inhibition of immobilized cell growth may occur as a result of diffusive transport limitation of product removal. When an acidogenic microorganism was immobilized in a model system, a higher acid concentration (lower pH) prevailed in the immobilized cell microenvironment than in the free solution outside the cell aggregate. Growth rates and growth yields substantially below those that would be anticipated under the bulk solution conditions were measured for

TABLE 3. Summary of autoradiographic data and immobilized cell growth rates

S_m (mM)	$z - b$ (μm)	b (μm)	d (μm)	$t_c + t_p$ (h)	a (μm)	μ (h^{-1})	μ* (h^{-1})
2.0	—[a]	7.5 ± 0.5	3	1	4 ± 3	—	—
5.0	49 ± 2	13 ± 1	4	11	9 ± 2	0.52 ± 0.14	0.5
12.0	128 ± 8	23 ± 7	3	25	20 ± 6	0.26 ± 0.11	0.3
16.0	40 ± 10	30 ± 2	4	11	28 ± 3	0.13 ± 0.05	0.2

[a] —, The pulse-fix labeling protocol used in this experiment did not enable measurement of z and μ. In addition, R_f and a were too imprecise to afford a meaningful estimate of μ*.

immobilized bacteria. The difference in the immobilized and bulk solution microenvironments was satisfactorily predicted by a simple model of reaction and diffusion in the microbial aggregate. Concomitant changes in growth kinetic parameters, which were shown to be governed by the acid concentration in suspension culture, were likewise adequately explained through such a model. In other words, once physical-chemical alteration of the microenvironment has been accounted for, immobilized and free-living cells appear to display a similar kinetic behavior. There is no evidence from this study for additional physiologic perturbation beyond that manifested in the local concentrations of substrate and product.

The results obtained in this investigation, in which we used a relatively inert immobilization support, certainly do not preclude the possibility of specific cell-support interactions that might alter cell behavior in the absence of microenvironmental differences. The potential biological effects of microbe-surface interactions, which may exist in some adsorption or entrapment immobilization systems, remains an interesting question for study. It will be necessary, however, in addressing this issue experimentally to definitively eliminate microenvironmental differences arising from physical-chemical mechanisms.

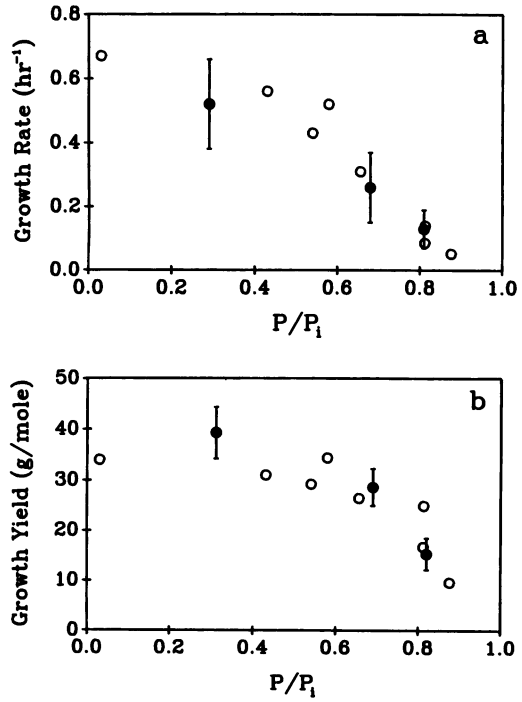

FIG. 7. Growth rates (a) and growth yields (b) of immobilized and free-living cells versus product concentration. Symbols: ○, free-living cells from batch and continuous cultures; ●, immobilized cells. The growth rates that are plotted are the purely autoradiographically determined values, μ.

Product inhibition arising from mass transfer limitation might be important in a variety of natural and applied systems. In addition to depressing the overall reaction rate and individual growth kinetic parameters, product inhibition could lead to shifted metabolic pathways and increased rates of cell lysis, degradation, and loss of viability. Together, these phenomena offer a possible explanation for some of the claims of altered behavior of immobilized cells, especially those taking the form of reduced growth yields and shifted pH optima. Wastewater treatment systems in which biofilms or aggregated microorganisms are used to carry out reactions that involve a pH change (e.g., nitrification, denitrification, and acetogenesis) are subject to product inhibition. To the extent that product inhibition decreases biomass formation, it may be beneficial in these applications. Product inhibition is most significant in waters that are poorly buffered. Furthermore, pH inhibition arising from mass transfer limitation is not effectively alleviated by the addition of neutralizing agents that are not diffusively transported (e.g., calcium carbonate). Mass transfer-limited product removal may play a significant role in the manifestation of dental caries. Acidic species generated in dental plaque from carbohydrates in foods are thought to promote demineralization of the tooth enamel and dentin (13). In these and other examples, a better understanding of the immobilized system hinges on an appreciation for the interaction between relevant physical-chemical mechanisms and intrinsic kinetic behavior.

ACKNOWLEDGMENTS

We extend thanks to Steven Karel and Peter Salmon for technical advice and assistance and to G. M. Homsy for the loan of equipment.

This study was supported by grant ECF-8519184 from the National Science Foundation.

LITERATURE CITED

1. **Arvin, E., and G. H. Kristensen.** 1982. Effect of denitrification on the pH in biofilms. Water Sci. Technol. **14**:833–848.
2. **Atkinson, B., J. Rott, and I. Rousseau.** 1977. Characteristics of unbuffered gel-immobilized urease particles. I. Internal pH. Biotechnol. Bioeng. **19**:1037–1063.
3. **Bailey, J. E., and T. C. Chow.** 1974. Immobilized enzyme catalysis with reaction-generated pH change. Biotechnol. Bioeng. **26**:1345–1357.
4. **Birkmann, A., F. Zinoni, G. Sawers, and A. Böck.** 1987. Factors affecting transcriptional regulation of the formate-hydrogenlyase pathway of *Escherichia coli*. Arch. Microbiol. **148**:44–51.
5. **Blanch, H. W., T. B. VickRoy, and C. R. Wilke.** 1984. Growth of procaryotic cells in hollow-fiber reactors. Ann. N.Y. Acad. Sci. **434**:373–381.
6. **Doran, P. M., and J. E. Bailey.** 1986. Effects of immobilization on growth, fermentation properties, and macromolecular com-

position of *Saccharomyces cerevisiae* attached to gelatin. Biotechnol. Bioeng. **28**:73–87.
7. **Evans, P. J., and H. Y. Wang.** 1984. Pigment production from immobilized *Monascus* sp. utilizing polymeric resin adsorption. Appl. Environ. Microbiol. **47**:1323–1326.
8. **Fletcher, M.** 1986. Measurement of glucose utilization by *Pseudomonas fluorescens* that are free-living and that are attached to surfaces. Appl. Environ. Microbiol. **52**:672–676.
9. **Gottschalk, G.** 1979. Bacterial metabolism. Springer-Verlag, New York.
10. **Jain, K. M., and R. C. Wagner.** 1980. Introduction to biological membranes, p. 216–218. John Wiley & Sons, Inc., New York.
11. **Karel, S. F., C. A. Briasco, and C. R. Robertson.** 1987. The behavior of immobilized living cells: characterization using isotopic tracers. Ann. N.Y. Acad. Sci. **506**:84–105.
12. **Karel, S. F., S. B. Libicki, and C. R. Robertson.** 1985. The immobilization of whole cells: engineering principles. Chem. Eng. Sci. **40**:1321–1354.
13. **Kleinberg, I.** 1977. Dental caries, p. 515–534. *In* W. A. Nolte (ed.), Oral microbiology, 3rd ed. C. V. Mosby Co., St. Louis.
14. **Mason, C. M., and J. B. Culvern.** 1949. Electrical conductivity of orthophosphoric acid and of sodium and potassium dihydrogen phosphates at 25°C. J. Am. Chem. Soc. **71**:2387–2393.
15. **Perry, R. H., and C. H. Chilton (ed.).** 1973. Chemical engineers' handbook, 5th ed. McGraw-Hill Book Co., New York.
16. **Pirt, S. J.** 1975. Principles of microbe and cell cultivation, p. 143–146. John Wiley & Sons, Inc., New York.
17. **Radovich, J. M.** 1985. Mass transfer effects in fermentations using immobilized whole cells. Enzyme Microb. Technol. **7**:2–10.
18. **Ramachandran, P. A.** 1975. Solution of immobilized enzyme problems by collocation methods. Biotechnol. Bioeng. **17**:211–226.
19. **Robinson, R. A., and R. H. Stokes.** 1955. Electrolyte solutions. Academic Press, Inc., New York.
20. **Salpeter, M. M., L. Bachmann, and E. E. Salpeter.** 1969. Resolution in electron microscopic autoradiography. J. Cell Biol. **41**:1–20.
21. **Siegrist, H., and W. Gujer.** 1987. Demonstration of mass transfer and pH effects in a nitrifying biofilm. Water Res. **21**:1481–1487.
22. **Szwerinski, H., E. Arvin, and P. Harremoës.** 1986. pH-decrease in nitrifying biofilms. Water Res. **8**:971–976.
23. **van Ginkel, C. G., J. Tramper, K. C. A. M. Luyben, and A. Klapwijk.** 1983. Characterization of *Nitrosomonas europea* immobilized in calcium alginate. Enzyme Microb. Technol. **5**:297–303.
24. **Weibel, E. R.** 1979. Stereological methods, vol. 1. Practical methods for biological morphometry. Academic Press, Inc., London.